J. Wind Eng. Ind. Aerodyn. 133 (2014) 146–149

Contents lists available at ScienceDirect

Journal of Wind Engineering and Industrial Aerodynamics

journal homepage: www.elsevier.com/locate/jweia

Effects of vortex shedding in arrays of long inclined flat plates and ramifications for ground-mounted photovoltaic arrays

Kurt Strobel*, David Banks[1]

CPP Inc., 1415 Blue Spruce Dr., Fort Collins, CO 80524, USA

ARTICLE INFO

Keywords:
Flexible structures
Inclined flat plate
Photovoltaic arrays
Vortex shedding

ABSTRACT

Many wind loading codes and standards define flexible structures as slender structures that have a fundamental natural frequency less than 1 Hz. This paper demonstrates that this is not a suitable threshold for small structures like ground-mounted arrays of photovoltaic panels because structures this small can experience both self-excitation and buffeting from upwind panels at frequencies well above this value during both serviceability and design wind events.

1. Introduction

Designers of ground-mounted photovoltaic (PV) arrays often use wind loading standards, such as ASCE 7, to calculate wind loads on their system. Many of these standards provide an arbitrary upper limit to define the natural frequency above which a structure becomes dynamically insensitive. In ASCE 7-05 and ASCE 7-10, that upper limit is 1 Hz.

Inclined flat plates have been shown to shed vortices at a frequency consistent with the Strouhal number (also known as reduced frequency) of around

$$St = \frac{fL}{U} = 0.15 \tag{1}$$

where f is the frequency of the shedding (Hz), U is the mean wind speed, and L is the characteristic length. Fage and Johansen (1927) found that vortex shedding occurred at a reduced frequency of $fL/U = 0.15$. This was for an inclined plate in free flow, i.e. there was no ground effect. Matty (1979) found that the reduced frequency of vortex shedding was typically near 0.15, but that it was influenced both by plate's proximity to the ground and by the angle of incidence of the wind.

Chen and Fang (1996) tested a beveled flat plate at a range of Reynolds numbers and concluded that a value of $St = 0.16$ was suitable for tilts (i.e. angles of attack) ranging from 10° to 90°, if L is the vertical projected height of the plate

$$L = C \sin(\theta) \tag{2}$$

where C is the chord length and θ is the tilt (see Fig. 1).

Smaller ground-mount PV solar racking systems often have chord lengths of less than 2 m. For a fixed-tilt system with a tilt of less than 30°, $L < 1$ m. This means that we can expect vortex shedding to create a peak in the turbulence and excitation spectra at 1 Hz for sustained wind speeds at panel height ($z \sim 2$ m) of under 7 m/s. This can be expected for any wind event bringing 3-second gusts of 15 m/s (35 mph) at a height of 10 m. Even for wider racking systems with chords of 4 m, the critical gust wind speed will be under 30 m/s (70 mph gusts).

A significant resonant response can be expected to result when the vortex shedding peak in the energy spectrum matches a natural frequency of the structural system. The severity will depend on the mode shapes and inherent damping of the racking system.

The design wind speed in ASCE 7–10 for most of the desert regions in the USA where these systems are being installed is 115 mph. In such a climate, the critical wind speed to have vortex shedding match the natural frequency can be expected to occur several times per year if the natural frequency is 1 Hz. This is the case even for systems with natural frequencies above the 1 Hz limit. Hence the guidance provided by wind loading codes can mislead the designer to dismiss possible dynamic issues.

To assess the potential severity of this issue, a series of boundary layer wind tunnel tests was conducted on scaled models of PV racking systems. The resulting dynamic wind load patterns were combined with a representative mode shape (twisting about the center chord, or "hinge moment", see Fig. 1) to evaluate the resulting dynamic response. This mode shape is a simplification of

* Corresponding author. Tel.: +1 970 221 3371.
E-mail addresses: kstrobel@cppwind.com (K. Strobel), dbanks@cppwind.com (D. Banks).
[1] Tel.: +1 970 690 6959.

http://dx.doi.org/10.1016/j.jweia.2014.06.013
0167-6105/

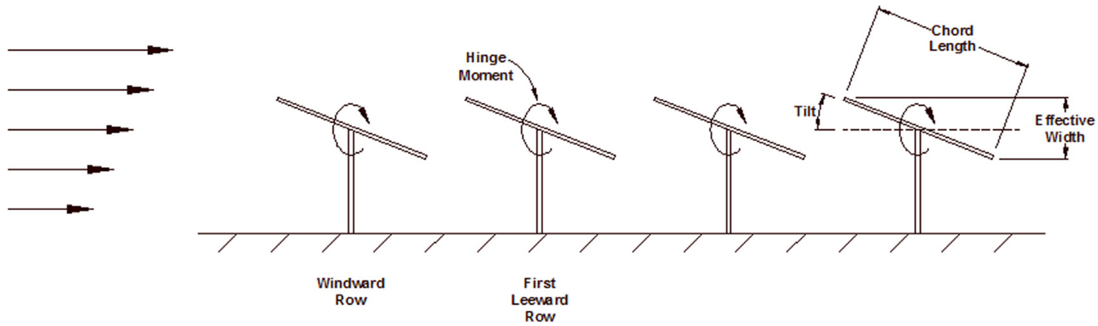

Fig. 1. Nomenclature for ground mount. Positive tilt shown.

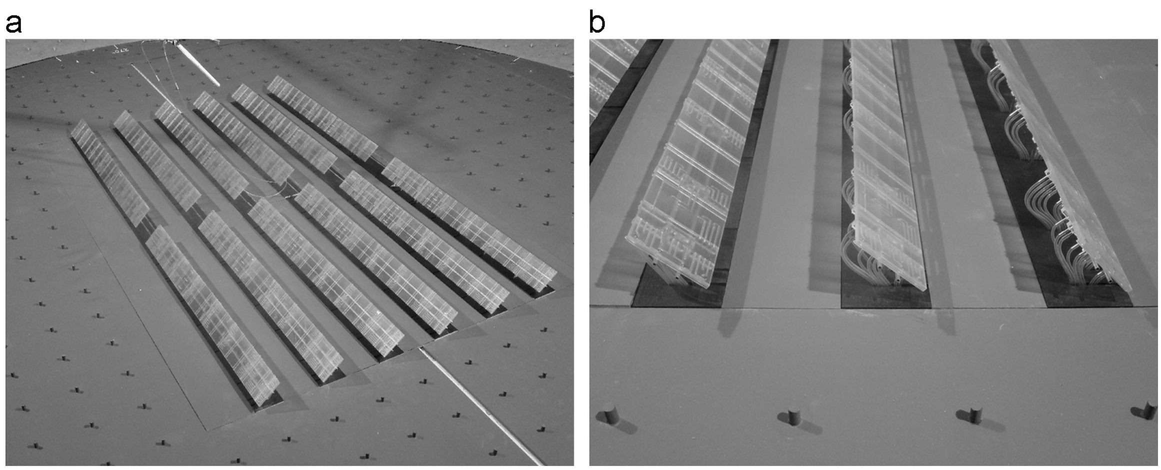

Fig. 2. Pictures of typical wind tunnel models.

mode shapes common to centrally supported ground mount-tracking systems. Results are presented for a range of damping ratios and natural frequencies that are representative of measurements on full scale trackers provided to CPP as part of proprietary studies.

2. Wind tunnel tests and data reduction

Pressure measurements were made at numerous locations over the entire surfaces of arrays of inclined flat plates in CPP's boundary layer wind tunnel in Fort Collins, Colorado. Fig. 2 shows pictures of a typical test model. These inclined flat plates were designed to model photovoltaic panels at scales of 1:30 to 1:50. A typical model included four pressure taps along the chord on both the top and bottom of the plate, with this pattern repeated many time along plates' length. For a given configuration of panel tilt, spacing and height, all wind directions were tested at 10° increments. For all tests, the height at which reference wind speed was measured by a pitot tube was 10 m in full scale. Sampling occurred at frequencies near 500 Hz. A "tubing correction" was applied to each times series to compensate for lower signal transmittance at higher frequencies.

The time series of individual pressure measurements were area integrated to calculate a time series of the hinge moment applied to each plate. In equation form, the hinge moment is given by

$$CM_h(t) = \frac{1}{A_{panel} l_{chord}} \sum_i Cp_i(t) A_i l_i \tag{3}$$

where A_{panel} is the area of the panel, l_{chord} is the chord length of the panel, $Cp_i(t)$ is the pressure coefficient at tap i, A_i is the tributary area assigned to tap i and l_i is the moment arm length of tap i. Note that $Cp_i(t)=p_i(t)/Q_{ref}$ where Q_{ref} is the average pressure measured by the pitot tube.

Power spectra, $S(f)$, were calculated from each time series of hinge moment using fast Fourier transform (FFT) techniques. The fluctuating (standard deviation) resonant hinge moment response was estimated from the excitation power spectra using Miles' approximation (Miles, 1954)

$$C\tilde{\mathbf{M}}_h = \sqrt{\frac{\pi}{4\zeta} f_o S(f_0)} \tag{4}$$

where f_o is the assumed natural frequency and ζ is the assumed inherent damping. Finally, the total response was calculated as

$$\mathbf{CM}_h = C\overline{M}_h \pm \sqrt{(g_b C\tilde{M}_h)^2 + (g_r C\tilde{\mathbf{M}}_h)^2} \tag{5}$$

where $C\overline{M}_h$ and $C\tilde{M}_h$ are the mean and standard deviation, respectively, from the hinge moment coefficient time series, g_b is the peak factor associated with so-called background excitation (g_b=3.5 was assumed for this paper), and g_r is the peak factor associated with the resonant fluctuations. For this paper, we applied a commonly used equation from Davenport (1964)

$$g_r = \sqrt{2\ \ln(f_0 T)} + \frac{0.5772}{\sqrt{2\ \ln(f_0 T)}} \tag{6}$$

where T is the reference time period, usually 3600 s (1 h).

3. Results and discussion

Fig. 3 illustrates typical power spectra of hinge moment coefficient, and shows that vortex shedding does not cause significant self-excitation of the hinge moment on the first row, but that it dominates the fluctuating load on the second row via buffeting.

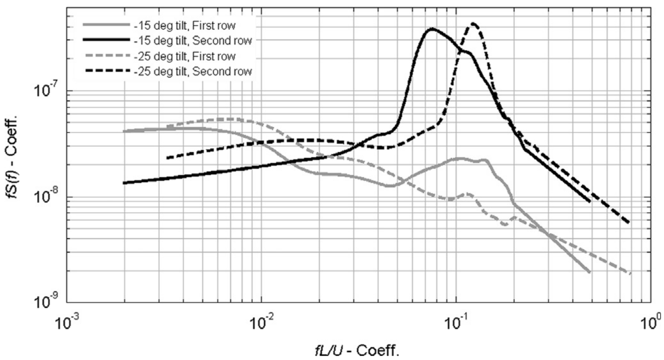

Fig. 3. Power spectra of hinge moment coefficient for $-15°$ and $-25°$ tilts.

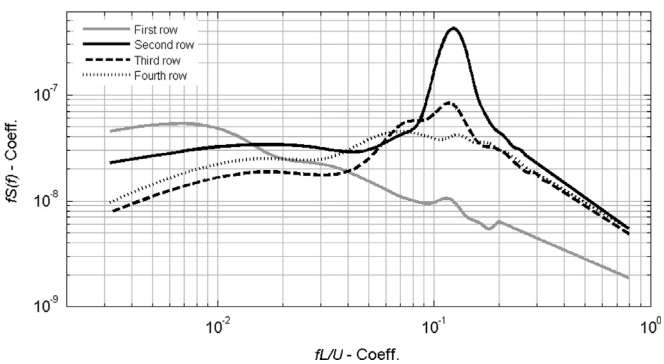

Fig. 4. Power spectra of hinge moment coefficient for $-25°$ tilt, winds normal to the rows, showing first four rows.

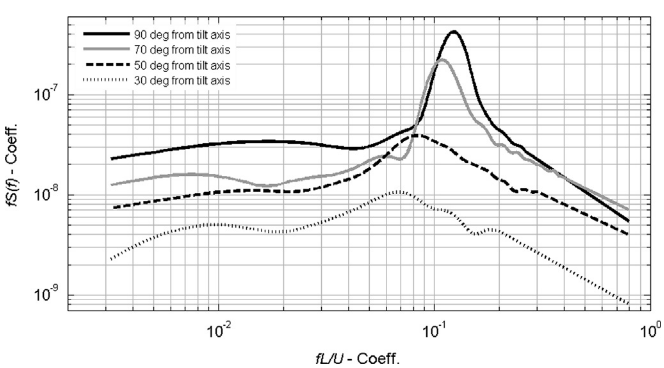

Fig. 5. Power spectra of hinge moment coefficient for $-25°$ tilt, second row, winds from varying direction.

Fig. 4 shows the decrease in the buffeting effect as the distance into the array increases. As previously discussed, the second row shows a dramatic peak near $fD/U=0.15$. The peaks in the third and fourth rows are less dramatic and occur at a lower reduced frequency. Though a bump at $St=0.15$ remains in all cases, a shoulder appears to the left and eventually takes over. This reduction in reduced frequency at which the spectral peaks occur is likely due to slowing of the wind by the array. As the mean wind speed slows, the periodicity of the vortices created by the windward panel slows down.

Fig. 5 shows the effect of wind direction relative to the tilt axis. The buffeting experienced by the second row is most substantial for wind normal to the tilt axis. As the direction becomes more parallel, the buffeting effect decreases. The sensitivity of the vortex shedding intensity to tilt angle and wind direction provides additional complexity for the designer of a tracking photovoltaic system.

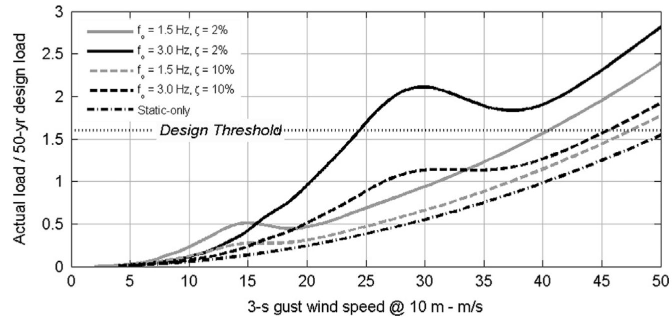

Fig. 6. First leeward row, tilt $=-15°$. Chord length $=2$ m. Open-country exposure assumed.

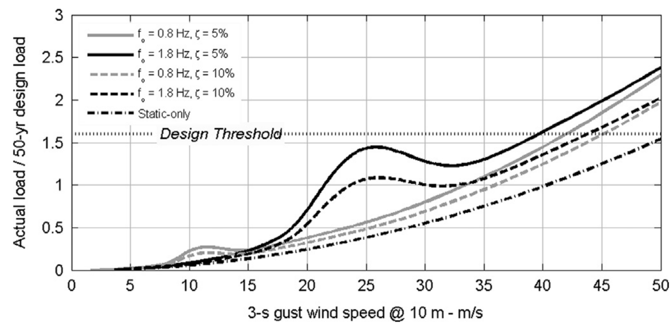

Fig. 7. First leeward row, tilt $=-25°$. Chord length $=3$ m. Open-country exposure assumed.

The spectra in Figs. 3–5, were provided as examples from a single "configuration". In other words, all spectra presented were measured using the same panel size, tilt axis height and row-to-row spacing. The effects of vortex shedding have been seen on all configurations that CPP has tested. The magnitude of self-excitation and buffeting vary mainly due to row spacing and tilt axis height. Additionally, the same phenomenon is seen for positive tilt angles.

Using Eq. (5), the dynamic response of a typical photovoltaic panel can be estimated due to exposure to the type of excitation shown in Figs. 3–5. Figs. 6 and 7 provide examples of such an estimate for a structure with varying natural frequency and damping ratio. Fig. 6 shows that the "static-only" load, i.e. the load expected without resonant response, is exceeded at lower wind speeds for all cases that include resonance. The mode shape associated with the natural frequency is assumed to have deflections that are similar to the deflections that would be produced by applying a hinge moment.

Figs. 6 and 7 also show the importance of the damping ratio. It should be noted that oftentimes the damping ratio of a photovoltaic structure that is designed to track sun's path is much higher than the 0.5–1% normally assumed for a steel structure. This increase in damping likely results from friction between the components of the tracking system. It should be strongly recommended that PV system designers perform measurements to determine the damping within their system rather than relying on nominal values associated with very different civil structures.

As a final note, Figs. 6 and 7 suggest the possible solution to wind-induced dynamics: reducing structure's natural frequency. While such a solution may create problems for withstanding design loads, it forces the peak dynamic response (as a ratio to background excitation) to occur at lower wind speeds such that the total response is diminished. This solution could be accomplished by using heavier and lower modulus materials. Such a solution may even reduce material costs, whereas the alternate solution of making the structure many more times rigid and light would likely incur exorbitant material costs.

4. Conclusions

These findings emphasize the importance of incorporating estimates of resonant loading on PV panels even if structure's natural frequencies are above 1 Hz. This is contrary to the guidance provided by ASCE 7 and elsewhere which treat structures with a natural frequency above 1 Hz as dynamically insensitive. As a result of this guidance, few designers or building officials consider dynamic effects of ground-mounted systems before they are built, only to later discover dynamic issues occurring at moderate wind speeds. We believe that it is urgent that a lower size limit be publicized for the use of the 1 Hz threshold, and that a different limit for small, slender structures be provided, preferably one that is a function of the size of the structure.

Acknowledgments

Yarrow Fewless managed the experimental work.

References

Chen, J.M., Fang, Y., 1996. Strouhal numbers of inclined flat plates. J. Wind Eng. Ind. Aerodyn. 61, 99–112.
Davenport, A.G., 1964. Note on the distribution of the largest value of random function with application to gust loading, Proceedings of the Institution of Civil Engineers, 28, pp. 187–196.
Fage, A., F.C. Johansen, 1927. On the flow of air behind an inclined flat plate of infinite span, In: Proceedings of the Royal Society of London, 116, pp. 170–197.
Matty, R.R., 1979. Vortex shedding from square plates near a ground plane: an experimental study, Masters thesis, Texas Tech University.
Miles, J.W., 1954. On structural fatigue under random loading. J. Aeronaut. Sci., 753.